An Investigation into the railway ballast dielectric properties using different GPR antennas and frequency systems

Fabio TOSTI[1]*, Luca BIANCHINI CIAMPOLI[2], Alessandro CALVI[2], Amir M. ALANI[1], Andrea BENEDETTO[2]

[1]School of Computing and Engineering, University of West London (UWL), St Mary's Road, Ealing, London W5 5RF, UK e-mail: Fabio.Tosti@uwl.ac.uk (*Corresponding author); Amir.Alani@uwl.ac.uk

[2]Department of Engineering, Roma Tre University, Via Vito Volterra 62, 00146, Rome, Italy e-mail: luca.bianchiniciampoli@uniroma3.it; alessandro.calvi@uniroma3.it; andrea.benedetto@uniroma3.it

Abstract

This paper presents an investigation into the relative dielectric permittivity of railway ballast using ground-penetrating radar (GPR). To this effect, experimental tests are carried out using a container (methacrylate material) of the 1.5 × 1.5 × 0.5 m dimensions. GPR systems equipped with different ground-coupled and air-coupled antennas and central frequencies of 600 MH, 1000 MHz, 1600 MHz and 2000 MHz (standard and low-powered antenna systems) are used for testing purpose. Several processing methods are applied to assess and compare the dielectric permittivity of the ballast system under investigation. Comparison of results identifies critical factors as well as antennas and central frequencies most suitable for the purpose.

Keywords: Ground-penetrating radar (GPR); Railway ballast; Non-destructive testing; Antenna frequency; Antenna systems; Relative dielectric permittivity.

1. INTRODUCTION

The use of ballast aggregates for the construction of railroads is massive in railway engineering and the effective assessment and health monitoring of their geometric, physical and mechanical properties is an issue of major concern in terms of safety of the operations and costs of of the rail asset management. The railway ballast usually consists of coarse aggregates with a relatively uniform grain size that are produced from crushed rocks, such as gravel, limestone, basalt or granite. Among the most important structural and functional tasks covered by the ballast aggregates, it can be cited i) the resistance to the vertical, lateral and longitudinal loads exerted on the sleepers; ii) the reduction of the maximum stress from the sleepers area to a minor stress level at the foundation and iii) the improvement of the water drainage across the whole track bed structure [1].

A track bed structure is made by a substructure (ballast, sub-ballast and subgrade), which lies underneath a superstructure (steel rails, fastening systems and sleepers). The cyclic loading exerted by the moving trains affects both of these main structural components, although the ballast and the sub-ballast layers are the structural components that are subject to the major deformations. This occurrence may cause potential segregation of the aggregates and the loss of the designed strength conditions.

The design thickness of a ballast and sub-ballast system ranges between 0.45 m and 0.75 m. These two layers can be found together in new and rehabilitated rail lines, whereas old rail infrastructures are mostly composed of only one layer of ballast above the subgrade [2]. Furthermore, new railroads are provided with a concrete slab or a geotextile at the sub-ballast – subgrade interface. On the contrary, these protective systems are absent from the oldest railways. This may be a serious concern in terms of the upward passage of the smallest clayey and silty particles from the subgrade by capillary actions. The progressive filling of the inter-particle voids within the ballast/sub-ballast layer by fine-grained materials may undermine the strength mechanisms between the aggregate particles. This occurrence is known as “fouling” and it can be due to several causes, as discussed by Selig et al. [3]. Mostly, the fouling occurrence may imply safety issues, such as the instability of the track, hence, it may lead to potential derailment of trains.

Visual inspections, punctual drillings and diggings are the traditional methods used for the monitoring and the assessment of ballast, all of which are performed at discrete intervals along the track. To this effect, it is worth mentioning the impossibility to interpret the causes of damage when using these techniques, if the causes are related to subsurface factors. In addition, it is impossible to provide continuous monitoring of the track

conditions. These methods are also time-consuming and labor-intensive, although they can provide very accurate information [4].

In view of the above, it is crucial to ensure the effective monitoring of the ballast aggregates as well as the early-stage detection of the main causes of damage in the construction, quality control and maintenance phases. This allows to optimise the maintenance expenses as well as to maintain the track stability and the desirable safety conditions.

The recent trend in railway engineering is to focus on the use of non-destructive testing (NDT) methods in order to perform rapid and non-intrusive inspections of the track bed. Within these methods, the optical-based two-dimensional (2-D) [5] and three-dimensional (3-D) [6] laser scanners and, mostly, the ground-penetrating radar (GPR) are worthy of mention. The GPR geophysical inspection tool is used in a wide range of application fields such as in planetary sciences [7], civil and environmental engineering [8], geology [9] and archaeology [10], forensics and public safety [11]. In the area of transport engineering, GPR has been used used mostly in: highway engineering [12], for the inspection of flexible (both bound [13 – 16] and unbound [17 – 19] layers) and concrete [20] pavements as well as in the monitoring of the subgrade soils [21, 22]. Applications of GPR can be also found in airfield engineering [23] and for the monitoring of critical infrastructures, such as bridges [24], [25] and tunnels [26].

The use of GPR in railway engineering has increased over the past 25 years. According to Roberts et al. [27], the first attempt of using GPR for the investigation of railways can be dated back to 1985 [28]. This study involved the use of ground-coupled antenna systems of 500 MHz central frequency mounted between the rails. The authors reported difficulties with the interpretation of the results due to the low resolution of the collected GPR scans. The use of higher investigation frequencies and air-coupled radar systems (mostly of 1000 MHz [29, 30]) has increased in the years following. Air-coupled antennas with a central frequency of 2000 MHz are being used more recently, and innovative frequency-based approaches have been developed accordingly [2, 31].

With regard to the assessment of the dielectric properties of the ballast aggregates, several studies can be mentioned. Clark et al. [1] performed a set of experiments in the laboratory environment to evaluate the dielectric properties of the ballast for a combination of dry/wet and clean/spent conditions. The authors argued that the best results may be achieved using low-frequency antennas. Sussman et al. [32] showed the importance

of the mineralogy of the ballast aggregates in interpreting their electromagnetic (EM) behaviour. Nevertheless, the authors emphasized also the relevance of the aggregates roughness and arrangement (within the track bed) as factors affecting the dielectric permittivity of the ballast/sub-ballast layer. A comprehensive review on the assessment of the EM properties of railway ballast can be found in [33].

In view of the non-uniqueness of the results above, this work focuses on analyzing the criticality of a number of parameters within the assessment of the dielectric permittivity of clean ballast aggregates. To this effect, a unique laboratory setup was built and a wide range of GPR antennas and frequency systems were used. The influence on the dielectric permittivity value of i) the type of radar system; ii) the antenna frequency; iii) the proposed data processing scheme; iv) the GPR method of data analysis and v) the arrangement of the ballast aggregates, is analysed in this study.

2. AIM AND OBJECTIVES

The main aim of this investigation is to identify critical factors as well as antennas and central frequencies most suited for the investigation of railway ballast.

To achieve this aim, the following objective are identified:

- to assess the dielectric permittivity of the ballast system under investigation (limestone ballast aggregates in clean conditions) using air-coupled GPR systems with different central frequencies as well as several processing methods
- to compare and analyse the results in order to single out the most suitable frequency of investigation, data processing scheme and methods for data analysis with respect to different scenarios of ballast aggregates arrangement.

3. METHODOLOGY

The geometric, physical and mechanical properties of the railway ballast aggregates are first assessed following the main international standards in the field.

The experiments are carried out in the laboratory environment on a methacrylate container, that is filled up and emptied three times with (same) ballast aggregates. To this effect, different scenarios are reproduced in terms of aggregates arrangement within the volume of the container used in this investigation.

GPR systems equipped with different ground-coupled and air-coupled antennas and central frequencies of 600 MH, 1000 MHz, 1600 MHz and 2000 MHz (standard and low-powered antenna systems) are used for testing purpose. A signal processing scheme is developed to filter out the useless information from the raw data. The relative dielectric permittivity of the bi-phase system (i.e., air-ballast aggregates) is computed using the time-domain signal picking (TDSP) technique, i.e., by the estimation of the wave propagation velocity within the investigated medium (e.g., [34]), across the full range of frequencies used. With regard to the air-coupled antenna systems, the surface reflection method (SRM) [35] and the volumetric mixing formula (VMF) methods are also applied for the same purpose.

4. THEORETICAL FRAMEWORK

4.1 GPR working principles

A GPR system is usually configured by one transmitting and one receiving antenna(s), a control unit, a data storage and a display unit. Overall, an EM impulse is emitted by the transmitting antenna towards the investigated surface. The signal is then reflected and scattered by the dielectric anomalies in the subsurface and collected by a receiving antenna. The properties of the materials can be estimated by several characteristics that are extracted from the signal such as the time delays, the amplitudes of the reflection peaks and the frequency modulations. A conventional analog-to-digital (A/D) converter is used to convert the extracted information in such a way that a real-time displaying of the data as well as additional processing can be performed. Ground-coupled or air-coupled antenna configurations are used as a function of the purposes and the types of the investigation. In more detail, the choice of the antennas is usually driven by the required penetration depth, the type of the soil to investigate and the (expected) size of the anomalies to detect. Fig. 1 shows a typical cross-section of a railway substructure and the relevant reflection pattern from a single GPR measurement, or A-scan. The A-scan provides a punctual “one dimensional” (1-D) information about the subsurface configuration. In Fig. 1, reflections are located at the electric discontinuities represented by the interfaces of the substructure layers. It is worth noting that the two-way travel time taken by the signal to cover the distance from the transmitter to the receiver is recorded in the vertical axis of an A-scan. This can be converted into distance units (usually given in centimetres) by knowledge/assumption of the wave propagation velocity in the medium, in order to display the depth of the signal reflections. On the contrary, the horizontal

axis of an A-scan represents the signal amplitude and it is usually given in Volts. A sequence of 1-D radar sweeps (A-scans) along the scanning line is used to create a 2-D matrix called radargram (B-scan). This is usually visualised in the real-time for immediate data interpretation. The vertical and horizontal axes of a B-scan represent the two-way travel time/depth information and the distance covered along the scanning line (usually given in meters), respectively.

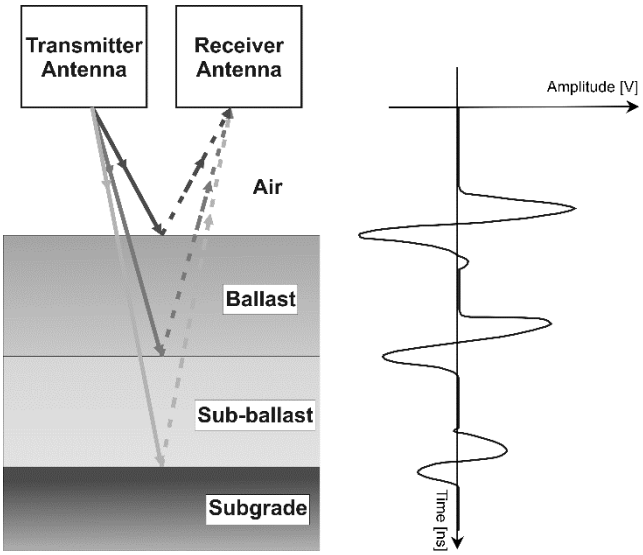

Fig. 1. Typical cross-section of a railway substructure and the relevant A-scan from a single GPR measurement.

4.2 Estimation methods of the relative dielectric permittivity

4.2.1 The time-domain signal picking technique

The first step for the assessment of the relative dielectric permittivity ε_r [-] of the bi-phase system reproduced in the laboratory environment (i.e., the ballast aggregates and the inter-particle air voids - from now on referred to as the "ballast system") is the calculation of the wave propagation velocity v [cm/ns] throughout a known thickness. This latter parameter represents the height h [cm] of a laboratory container filled up with ballast aggregates, as it is detailed further in Section 5.2. Hence, it is possible to estimate $v = 2h / \Delta t$ after measuring the time delay Δt [ns] between the two relevant reflection pulses of the GPR signal collected in the laboratory (i.e., the reflection pulses related to the surface and the bottom of the "ballast system"). The relative dielectric permittivity ε_r is therefore computed by working out the above expression of v into the following equation:

$$\varepsilon_r=(c_0/v)^2 \quad (1)$$

where c_0 is the speed of light in the free space [cm/ns]. This method (from now on referred to as "time-domain signal picking" (TDSP) method) is used in this study for the estimation of the permittivity using the full set of GPR systems and antenna frequencies available.

4.2.2 The surface reflection method

The surface reflection method (SRM) [35] allows for the evaluation of the relative dielectric permittivity ε_r [-] by comparison between specific reflection amplitudes as follows:

$$\varepsilon_r=\left(\frac{1+A_0/A_{\mathrm{PEC}}}{1-A_0/A_{\mathrm{PEC}}}\right)^2 \quad (2)$$

where A_0 [V] is the maximum absolute value of the signal amplitude reflected at the interface of the air/ballast surface; A_{PEC} [V] is the maximum absolute value of the amplitude reflected by a metal sheet placed at the bottom of the ballast system and larger than the antenna footprint (e.g. [36, 37]). This is defined as the effective area illuminated by the antenna on the investigated surface [38]. The main function of the metal plate is to act as a perfect electric conductor (PEC) preventing from unwanted reflections from the subsurface underneath the metal sheet and allowing for the complete reflection of the signal.

It should be noted that the above formulation relies on the assumptions of i) homogeneity of the investigated material, ii) negligibility of the electrical conductivity of the material and iii) plane wave approximation.

4.2.3 The volumetric mixing formulae

The volumetric mixing formula (VMF) theoretical model [39] is used to compute the dielectrics of the "ballast system" by assuming a multi-phase configuration of the investigated medium. The implementation of this method requires the knowledge of the relative dielectric permittivity value $\varepsilon_{r,i}$ [-] of each i^{th} phase component of a mix with n phases as well as the relevant volumetric fraction φ_i (the sum of which is equal to 1). The linear combination of these parameters provides the following relationship:

$$\varepsilon_r^{\alpha} = \sum_{i=1}^{n} \varphi \varepsilon_{r,i}^{\alpha} \quad (3)$$

where α is a geometrical fitting parameter varying between +1 and -1 [40, 41] and dependent on the inner structure of the investigated medium [42]. In this study, a value of 0.5 is assigned to the α factor (e.g., 43, 44).

Given this assumption, the VMF expressed by Eq. (3) is known as the complex refractive index model (CRIM) [39].

The relative dielectric permittivity values of the single multi-phase components are derived from the literature [45] and no frequency dependence is considered in this study. The permittivity of the ballast aggregates (i.e., limestone aggregates), the methacrylate base of the tank and the air are here assumed equal to 6.50, 4.00 and 1.00, respectively.

4.3 The data processing scheme

A data processing scheme is applied to the raw GPR signals as a sequence of four steps, namely, a) time-zero correction; b) signal stacking; c) zero-offset removal and d) band-pass filtering [46, 47]. The acquisition of the GPR traces is carried out in static conditions such that the data processing was applied to A-scan data outputs (e.g. Fig. 1). Fig. 2 reports the used processing scheme and the signal outputs at each of the aforementioned four steps in the case of the 1000 MHz central frequency of investigation.

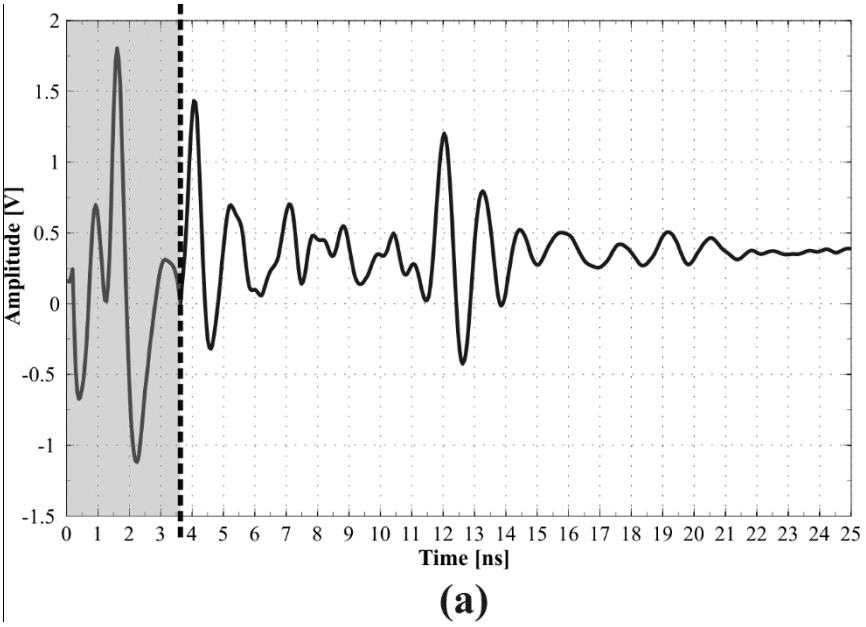

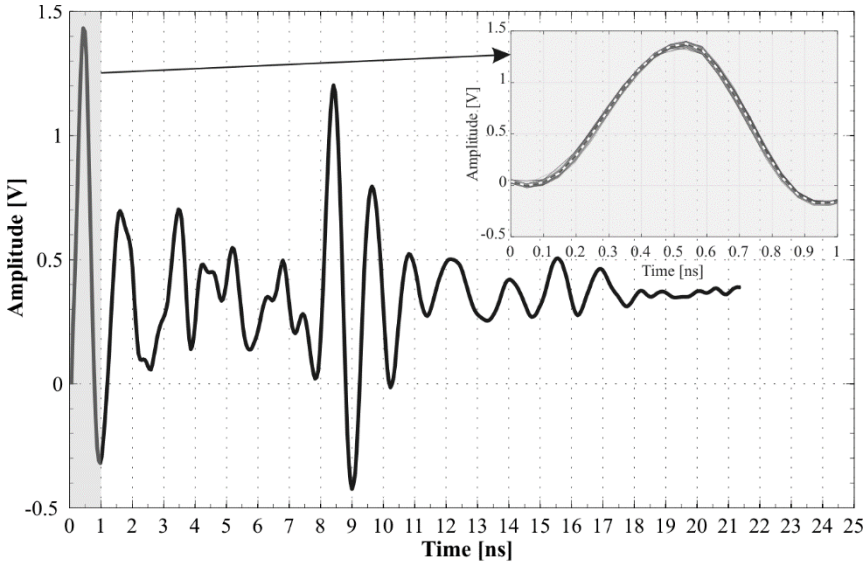
Amplitude [V]
Time [ns]
Amplitude [V]
Time [ns]

(b)

197

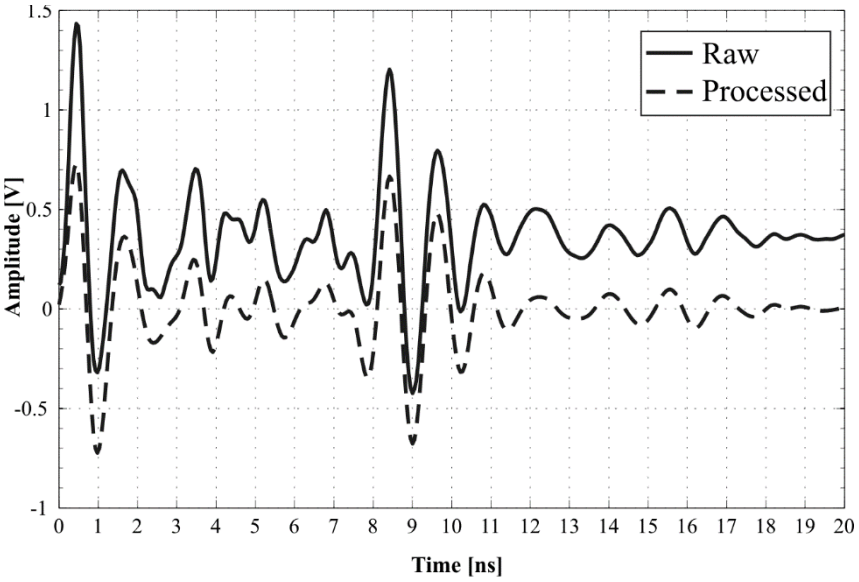
Raw
Processed
Amplitude [V]
Time [ns]

(c)

198

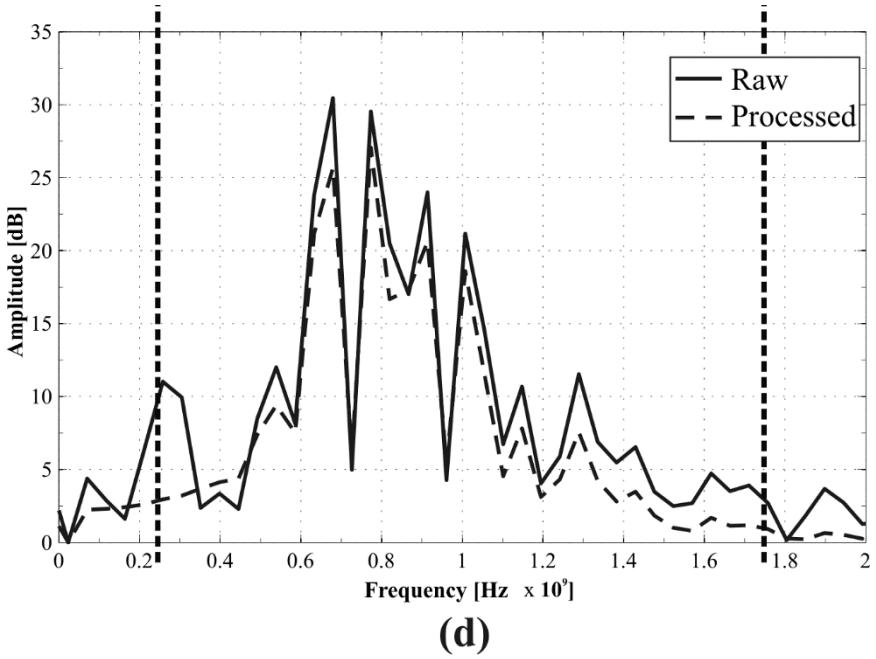

Fig. 2. Data processing scheme and 1000 MHz GPR outputs obtained after filtering with the time-zero correction (a); the signal stacking (signal stretch "0 ns -1 ns" magnified at the upper right corner) (b); the zero-offset removal (c) and the band-pass filtering (d).

The time-zero correction filter (Fig. 2a) is first applied to filter out all the useless reflections coming from the inner of the GPR apparatus as well as to set the zero-time at the zero-amplitude point between the negative and the positive peaks (i.e., the direct wave: the interface between the air and the railway ballast surface). This choice is motivated by the high stability of this point across a wide range of diverse surfaces and the relative ease of identification [48]. Inner reflections are identified for each GPR system by comparison between the signals collected at the various scenarios of ballast aggregates. Hence, the initial common parts of the signals (i.e., from the source point to the zero-amplitude point) are related to the reflections from the apparatus and filtered out. In the second step, the signal is averaged (stacked) over 100 traces according to the ASTM D6087-08 standard test method [36]. Stacking a number of traces collected at the same position increases the contribution coming from the target medium, whereas it reduces the random noise. Fig. 2b shows the average signal and the traces collected within the signal stretch "0 ns – 1 ns" of the time window (magnified at the upper right corner of the figure). The white dotted line in the magnified area of Fig. 2b represents the stacked signal and shows a relatively low variability of the traces collected. A zero-offset removal is subsequently applied such that an A-scans signal with a mean equal to zero is achieved (Fig. 2c). Following this step, a

band-pass filtering is applied to the signal considering a pass bandwidth of 1.5 times the central frequency of investigation with lower (high-pass filter) and upper (low-pass filter) boundaries evenly distributed around the central frequency [49, 50]. In view of this, Table 1 lists the high-pass and low-pass filters applied for each central frequency of investigation used in this study.

Table 1 High-pass and low-pass filters applied across the whole set of central frequencies of investigation used in this study.

	Central frequency [MHz]			
	600	1000	1600	2000
High-pass filter [MHz]	150	250	400	500
Low-pass filter [MHz]	1050	1750	2800	3500

The frequency spectra in Fig. 2(d) represent the band-pass filtering in the case of the 1000 MHz central frequency of investigation, These are obtained after the application of the Fast-Fourier Transform (FFT) to the relative time-domain signals.

From now on, the GPR signals subject to the aforementioned data processing scheme will be referred to as "processed" GPR signals as opposed to the "raw" GPR signals.

5 EXPERIMENTAL FRAMEWORK

5.1 Experimental design

The experimental design is focused on the analysis of the EM behaviour of clean limestone ballast aggregates in dry conditions. A laboratory setup is arranged for testing the combination of differing factors, namely, i) the type of radar system; ii) the antenna frequency; iii) the proposed data processing scheme; iv) the GPR method of data analysis; v) the arrangement of the ballast aggregates. Tests are carried out in static conditions and all the analyses were focused on the A-scan data outputs (e.g. Fig. 1). A number of preliminary analyses are performed to investigate into the footprints of all the available radar systems [36, 37]. To this effect, the testing

conditions are reproduced using the GPR systems and the available PEC only. The effective areas illuminated by the antennas on the PEC are determined following the manufacturer's recommendation on the systems' beam of radiation and after double-checking the signal disturbance by practical tests. These provide a gradual approach of a metallic reflector from the edge to the centre of the PEC while measuring with the GPR systems. The footprint boundaries are therefore determined when a disturbance to the signal is noticed (i.e., the signal is subject to edge effects). In view of the above framework, the largest dimension of the footprint at the PEC surface turns out to be ~150 cm and it is taken as the benchmark for the side of the container. This investigation is useful for the design of the dimensions of the container in order to assume the surveyed medium as horizontally infinite with negligible border effects.

5.2 Tools and equipment

Ground-coupled and air-coupled GPR antenna systems [50], manufactured by IDS Georadar (Fig. 3), are used for testing purposes. The RIS 99-MF Multi Frequency Array Radar-System is equipped with 600 MHz and 1600 MHz central frequency antennas. The system collects data by means of four channels, i.e., two mono-static and two bi-static. In this study, only the 600 MHz and 1600 MHz mono-static channels are used for data collection. A time window of 40 ns is used for the acquisition of the signal. In addition, three air-coupled GPR systems equipped with central frequency antennas of 1000 MHz (RIS Hi-Pave HR1 1000) and 2000 MHz (RIS Hi-Pave HR1 2000 and RIS Hi-Pave HR1 2000NA) are used. Time windows of 25 ns and 15 ns were set for, respectively, the 1000 MHz and the 2000 MHz GPR systems. It is worth emphasizing that the aforementioned time windows are set according to the manufacturer's recommendation [e.g., 21, 51, 52]. Proper combination of time window and sampling interval is mandatory to avoid over-/under-sampling of the signal collected, hence to modify/lose information [53]. With regard to the 2000 MHz antenna systems, both a standard version of the horn antenna for the European market and a low-powered version for the North-American (NA) market are used. In this regard, it is known that manufacturers must comply with different regulations about the power emission limit as per the country's specific needs [54]. The challenge is mostly in countries like the United States where the threshold for the maximum power emission is very low. Due to this lower radiative power, this type of GPR systems exhibit worst performances in terms of signal-to-noise (SNR) ratio [55]. It is therefore

important to test and compare the results to check the viability of low-powered GPR systems in assessing the dielectrics of railway ballast.

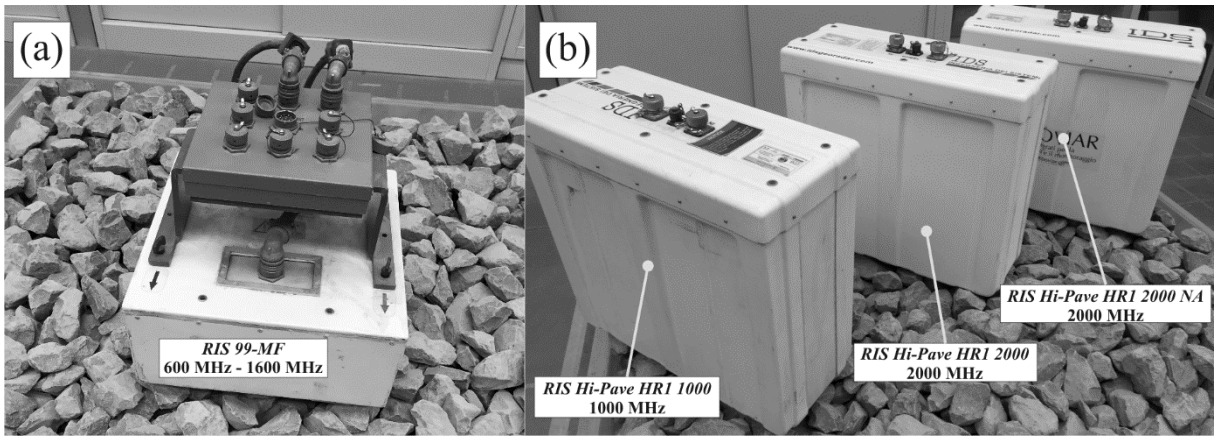

Fig. 3. GPR equipment used for testing purposes: RIS 99-MF ground-coupled multi-channel GPR system (a), and RIS Hi-Pave air-coupled antenna systems (1000 MHz, 2000 MHz and 2000 MHz (NA)) (b).

A square-based methacrylate tank is used for testing purposes (Fig. 4). The container has outer base side and height of, respectively, 1.55 m and 0.55 m, and inner dimensions of 1.47 m (side of the base) and 0.48 m (height). A 2 m × 2 m copper sheet PEC is laid underneath the container, thereby allowing for the full reflection of the EM waves propagating through the "ballast system". It is also worth noting that the dimensions of the investigated volume are designed to comply with the typical sizes of ballast layers in rail track beds.

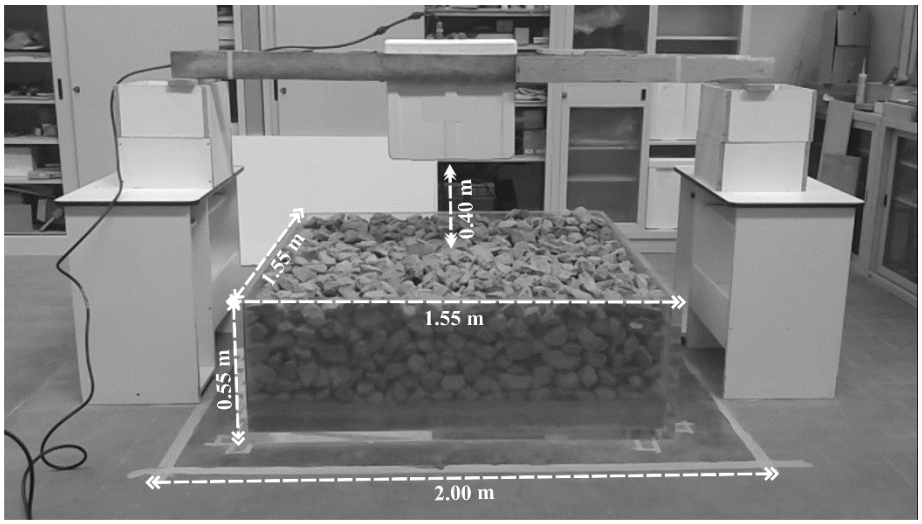

Fig. 4. Experimental setup for the measurements carried out in the laboratory with an air-coupled antenna system.

5.3 Materials and laboratory testing

Limestone ballast aggregates, typically used for the construction of ballasted railroads, are utilised for testing purposes. Prior to the GPR tests, a thorough assessment of the main geometric, mechanical and physical properties of the ballast aggregates is carried out according to the EN 13450:2002/AC:2004 standard [56]. In addition to this standard, further standard test methods for the assessment of the percentage of voids [57] and the water content [58] are followed. All of the above properties are listed in Table 2.

Table 2 Main properties of the limestone ballast aggregates assessed by using standard test methods.

Ballast property		Standard		Reference unit	Value	Class
Geometric	Grain size	EN 13450:2013 [45]	EN 933-1:2012 [59]	% passing vs. sieve size (mm): 80 -63 -50 -40 -31.5 – 22.4	100 – 100 -79.9 – 30.6 – 1.2 – 0.3	A
	Fine particles content		EN 933-1:2012 [59]	% passing vs. sieve size (mm): 0.063	0.5	A
	Particle length		EN 933-4:2008 [60]	%	5.5	B
	Shape index - *SI* -		EN 933-4:2008 [60]	%	20.0	SI_{20}
Mechanical & physical	Resistance to fragmentation - LA_{RB} -		EN 1097-2:2010 [61]	%	20.0	LA_{RB} 20
	Particle density - ρ_s -		EN 1097-6:2013 [62]	g/cm^3	2.8	/
	Percentage of voids - φ -	EN 1097-3:1998 [57]		%	41.0	/
	Water content - *w* -	CEN ISO/TS 17892-1:2005 [58]		%	0.2	/

One test is carried out using the ground-coupled multi-frequency radar system, where 100 traces are collected for each of the aforementioned frequencies of investigation.

Calibration measurements complying with [36] and [49] are performed for the three air-coupled systems. To this effect, a reference distance of 0.40 m is set between the PEC and the base of the GPR apparatus. The same distance is maintained between the base of each air-coupled GPR and the surface of the ballast system. In view

of the roughness of the ballast aggregates, these have been contained beneath the height of the container, which is taken as the benchmark for the height of the "ballast system". Three main scenarios of arrangement of the ballast aggregates are reproduced in the laboratory by filling up and emptying the container. For each scenario, the full set of air-coupled GPR systems are used and 9 tests are performed.

6 RESULTS AND DISCUSSION

6.1 Ground-coupled antenna systems

The proposed processing scheme is applied to the raw data. Therefore, the dielectric permittivity values of the "ballast system" are computed for both the raw and the processed data using the TDSP technique. Both the 600 MHz and the 1600 MHz mono-static channels are considered (Fig. 5).

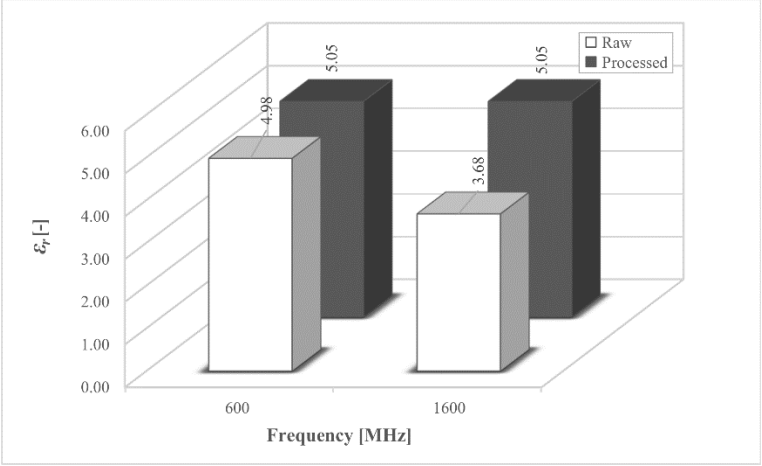

Fig. 5. Raw and processed values of the relative dielectric permittivity for the acquisitions carried out with the 600 MHz and 1600 MHz central-frequency antennas.

It is clear how the main difference between the raw and the processed data is in the case of the higher frequency. To this effect, if the following expression is considered for the incidence of the residuals ξ [%] (i.e, the percentage ratio of the difference between the raw (ε_{raw}) and the processed (ε_{proc}) dielectrics, and the raw value of the dielectric permittivity, taken as the reference):

$$\xi\ [\%] = \left(\frac{\varepsilon_{raw} - \varepsilon_{proc}}{\varepsilon_{raw}}\right) 100 \tag{4}$$

the values of ξ [%] are equal to 37.18% and 1.39% for, respectively, the 1600 MHz and the 600 MHz central frequencies. The application of the proposed data processing scheme leads to identical values of dielectric

permittivity. Nevertheless, it is worth noting how the processed values of relative dielectric permittivity are 1.0÷1.5 units higher than the dielectrics of similar materials, as indicated in several literature research [1, 31, 32]. Therefore, it can be argued that this antenna type is not well suited for the purpose of this study (i.e, the assessment of the dielectric permittivity of limestone railway ballast in clean conditions) and, in general, the complex material configuration can affect proper data collection with ground-coupled antenna systems. A reasonable motivation for this occurrence may be related to the effects of ringing. As it was observed by Narayanan et al. [63], it was indeed difficult to maintain the GPR apparatus during the tests within one eighth of the wavelengths of the two antennas above the rough surface of the ballast aggregates at the top of the container [64]. In this case, the low directivity of the ground-coupled antennas makes these systems more sensitive to the coarse grain size of the aggregates as well as to the edge effects, which may both affect the permittivity value [65].

6.2 Air-coupled antenna systems

Fig. 6 shows the values of the permittivity computed as a combination of each of the three air-coupled systems and the three scenarios of "ballast system". These dielectrics are derived from both the raw and the processed signals using the TDSP technique. For the sake of comparison, the bar graph of the relative dielectric permittivity calculated using the VMF model is also added. This equals 3.64 and it is obtained by substituting the values of the multi-phase components given in Section 4.2.3 into Eq. (3).

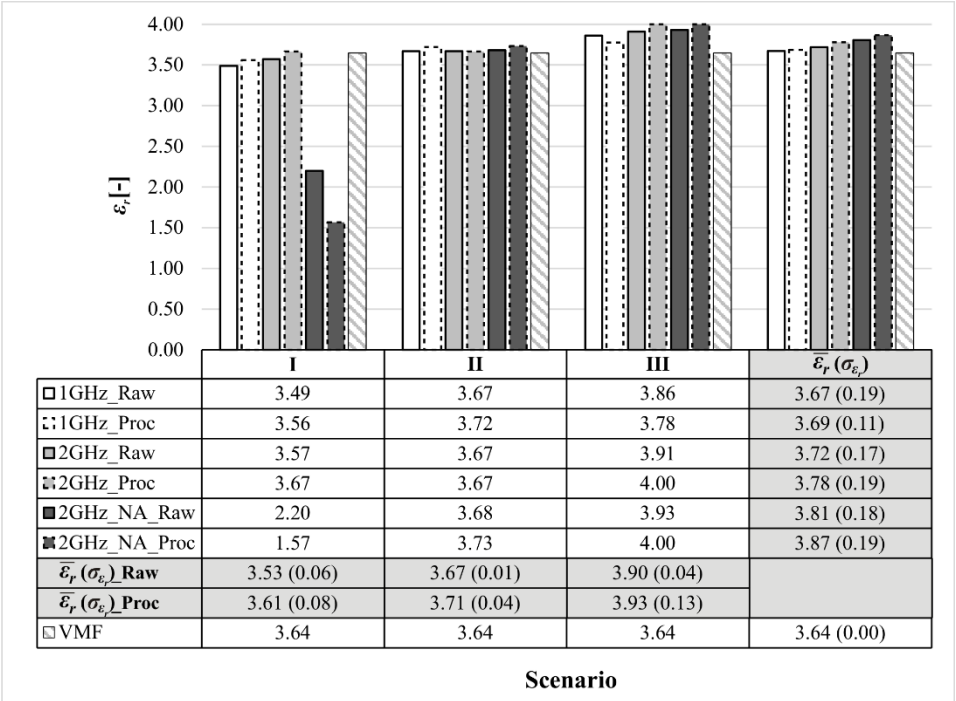

	I	II	III	$\overline{\varepsilon_r}\,(\sigma_{\varepsilon_r})$
1GHz_Raw	3.49	3.67	3.86	3.67 (0.19)
1GHz_Proc	3.56	3.72	3.78	3.69 (0.11)
2GHz_Raw	3.57	3.67	3.91	3.72 (0.17)
2GHz_Proc	3.67	3.67	4.00	3.78 (0.19)
2GHz_NA_Raw	2.20	3.68	3.93	3.81 (0.18)
2GHz_NA_Proc	1.57	3.73	4.00	3.87 (0.19)
$\overline{\varepsilon_r}\,(\sigma_{\varepsilon_r})$_Raw	3.53 (0.06)	3.67 (0.01)	3.90 (0.04)	
$\overline{\varepsilon_r}\,(\sigma_{\varepsilon_r})$_Proc	3.61 (0.08)	3.71 (0.04)	3.93 (0.13)	
VMF	3.64	3.64	3.64	3.64 (0.00)

Fig. 6. Values of the relative dielectric permittivity computed using the TDSP and the VMF methods for the acquisitions made with the 1000 MHz, 2000 MHz and 2000 MHz (NA) central-frequency antennas.

Overall, the permittivity values agree with the dielectrics of the same material as indicated in the literature [1, 31, 32]. Exceptions are the permittivity values (both raw and processed) computed using the TDSP technique within the first scenario of aggregates arrangement with the 2000 MHz (NA) antenna. Hence, these outliers are excluded from the statistics.

With regard to the dielectrics assessed with the TDSP technique, low peaks of variability are obtained for the whole set of the frequencies within each single scenario (i.e., $\sigma_{\varepsilon_r} = 0.01 \div 0.13$, if the minimum and the maximum values of the standard deviation is considered). On the contrary, higher peaks are found if each frequency f_j across the three i^{th} scenarios s_i (i.e., $\sigma_{\varepsilon_r} = 0.11 \div 0.19$) is taken into account. Thereby, it can be argued that the variation in the arrangement of the ballast aggregates (i.e., moving horizontally across the rows in Fig. 6), may affect the computed values of permittivity of the "ballast system" more than using differing frequencies of investigation across the same scenario (i.e., moving vertically across the columns in Fig. 6). Let us compare the three scenarios to three different sections of railway ballast layers that can be usually investigated along the rail track in the real-life conditions. Also, let us interpret the dielectrics found for the three antenna frequencies as the result of GPR data collected at the same i^{th} section (scenario) using a multi-

355 frequency antenna. The found standard deviations of the dielectrics mean that the arrangement of the
356 aggregates has a higher impact on the value of the permittivity than the used central frequency (within the
357 range of frequencies here available). This may be reasonably due to the twofold effect of the roughness at the
358 interface between the air and the ballast as well as to the arrangement of the aggregates throughout the thickness
359 of the "ballast system".
360 The impact made on the value of the permittivity by the use of different frequencies across the three reproduced
361 scenarios is represented by the trend of the average permittivity $\overline{\varepsilon_r}$ in the fourth grey column of Fig. 6. In
362 general, we can argue that the higher the central frequency of investigation, the larger the value of the
363 permittivity. To this effect and with regard to the processed data only, $\overline{\varepsilon_r}$ ranges from 3.69 (i.e., 1000 MHz) up
364 to 3.78 (i.e., 2000 MHz) and 3.87 (i.e., 2000 MHz (NA)).
365 Concerning the applied data processing scheme and its effect on the assessment of $\boldsymbol{\varepsilon_r}$, it is observed that the
366 average permittivity values $\overline{\varepsilon_r}$ of the processed data are slightly higher than the raw data. This occurs in both
367 the average dielectrics computed across the i^{th} scenario s_i investigated (same frequency: $\overline{\Delta\varepsilon_{\text{r proc-raw}}}$ = 0.2÷0.6;
368 i.e., fourth grey column in Fig. 6) and the j^{th} frequencies f_j (same scenario: $\overline{\Delta\varepsilon_{\text{r proc-raw}}}$ = 0.3÷0.8; i.e., two grey
369 rows in Fig. 6) used. To this effect, Fig. 7 shows the incidences of the residuals (Eq. (4)) computed between
370 the processed and the raw data for any combination of s_i and f_j. These results confirm that the proposed
371 processing scheme returns mostly higher values, with residual percentages not exceeding ± 3%.
372

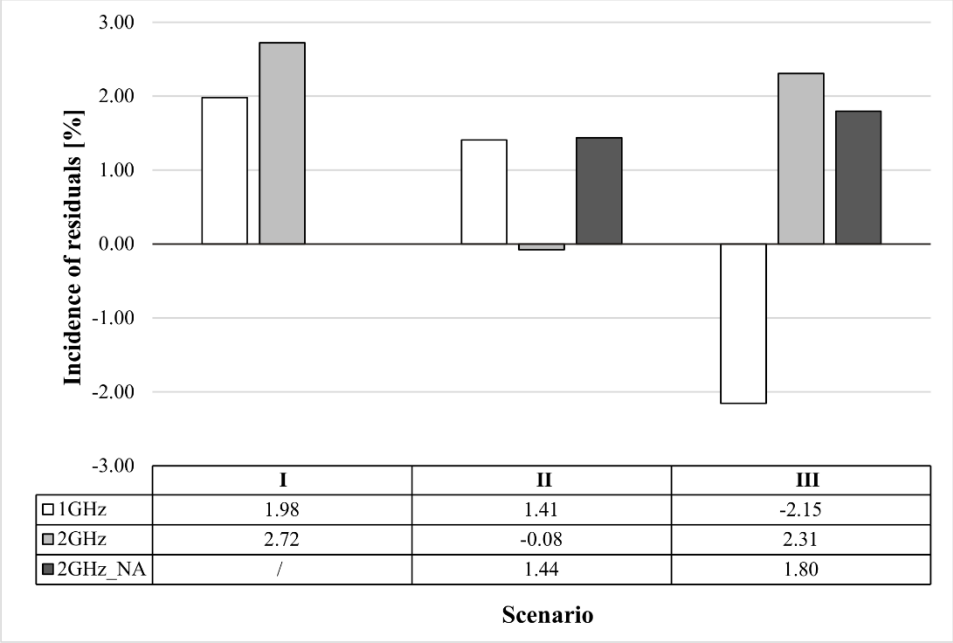

	I	II	III
1GHz	1.98	1.41	-2.15
2GHz	2.72	-0.08	2.31
2GHz_NA	/	1.44	1.80

373

Fig. 7. Incidence of the residuals between the processed and the raw permittivity data computed using the TDSP technique.

With regard to the GPR methods of data analysis, Fig. 8 reports the incidences of the residuals between the processed values of dielectrics, computed using the TDSP technique, and the relative dielectric permittivity value of 3.64 calculated by the VMF theoretical method. Overall, it can be seen how the permittivity assessed by the VMF is lower than the dielectrics derived from the application of the time-domain-based technique. An exception is the ε_r value calculated using the 1000 MHz antenna for the first scenario. Furthermore, lower mismatches are observed in the case of the 1000 MHz antenna, whereas the use of the 2000 MHz antennas returns broadly higher differences (with the exception of the 2000 MHz antenna in the second scenario of aggregates arrangement). This is summarized by the average values of the incidences $\bar{\zeta}_j$computed across the various scenarios s_i investigated (i.e., each frequency in the fourth grey column in Fig. 8). Furthermore, it can be seen that the low-powered antenna system returns the highest differences in terms of permittivity estimate between the TDSP and the VMF techniques. Fig. 9 reports the comparison between the processed values of dielectrics, computed using the TDSP technique, and the corresponding relative dielectric permittivity values obtained with the SRM approach. For the sake of comparison, the bar graphs with the VMF permittivity estimations are also included. It is evident that the SRM provides values of ε_r lower than the TDSP technique. Thereby, it shows to be unsuitable for the assessment of the dielectric permittivity of railway ballast layers within the analysed domain of investigation (i.e., the 3-D volume defined by the investigated "ballast system"). This result may be reasonably due to a higher sensitivity of the SRM towards the roughness of the ballast aggregates at the interface between the air and the "ballast system" in combination with the high inhomogeneity of the material throughout the investigated domain. Indeed, the former occurrence has an impact on the amplitude A_0 in Eq. (2), whereas the latter condition affects the major assumption of material homogeneity. This is confirmed by the highest dielectrics obtained with the SRM in the case of the 1000 MHz central frequency (i.e., $\overline{\varepsilon_{r\,1GHz}}$ = 2.56 against $\overline{\varepsilon_{r\,2GHz}}$ = 1.74 and $\overline{\varepsilon_{r\,2GHz\_NA}}$ = 1.66). As the wavelength λ_{1GHz} is higher than the wavelength λ_{2GHz} of the 2000 MHz GPR systems (according to the quarter of wavelength criterion [66]: λ_{1GHz}= 7.5 × 10^{-2} m; λ_{2GHz}= 3.75 × 10^{-2} m), hence, the effects of the inhomogeneity of the

system on the estimated value of dielectric permittivity are lower. In view of this, dielectrics closer to those obtained with the peak-to-peak (TDSP) estimation are reached.

It is important to note that the inhomogeneity of the ballast is a critical issue across all the applied GPR methods of data analysis. However, the effects of this condition in the application of the TDSP and the VMF approaches turn out to be more contained. Firstly, in the TDSP method the estimation of the wave propagation velocity v across the thickness of the whole "ballast system" seems to limit the effects of the material inhomogeneity. Secondly, the assumption of $\alpha = 0.5$ in the VMF theoretical model of Eq. (3) turns out to be a good trade-off for representing the inner structure of the investigated medium.

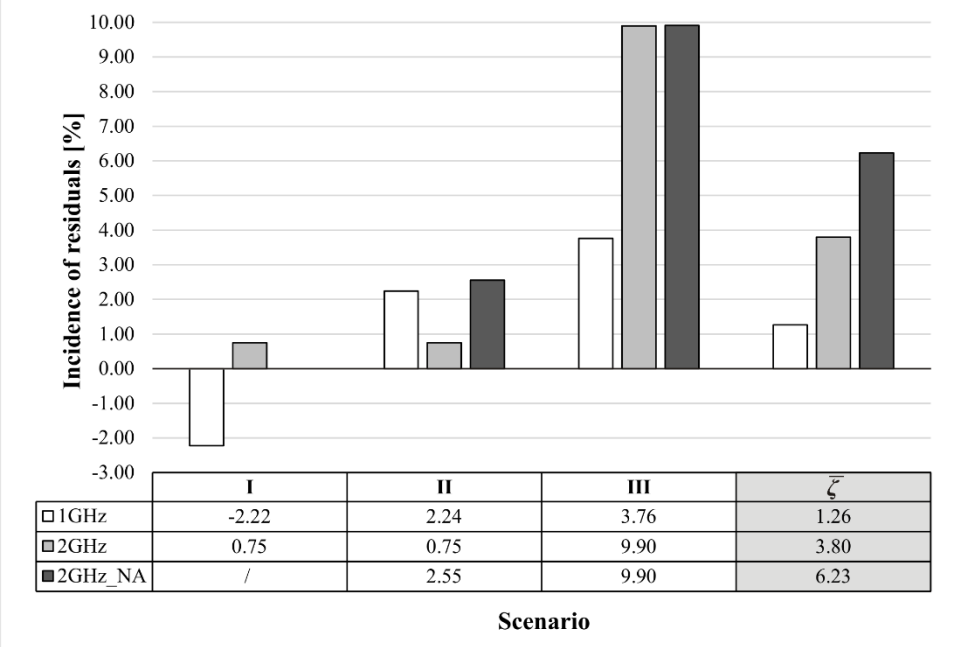

	I	II	III	$\bar{\zeta}$
1GHz	-2.22	2.24	3.76	1.26
2GHz	0.75	0.75	9.90	3.80
2GHz_NA	/	2.55	9.90	6.23

Fig. 8. Incidence of the residuals between the processed permittivity data computed using the TDSP technique and the dielectric permittivity calculated by the VMF model.

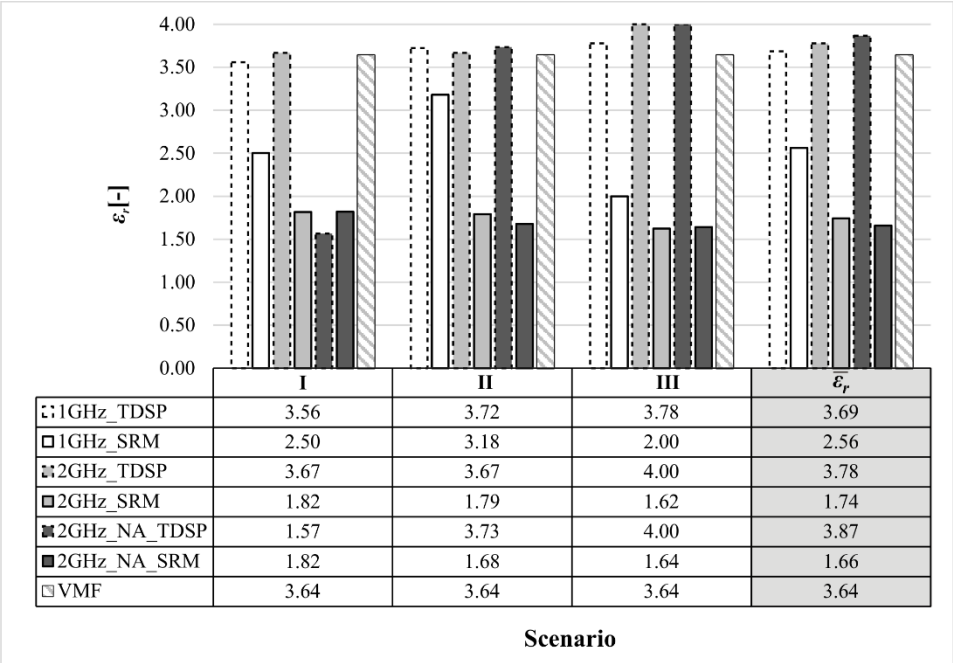

	I	II	III	$\overline{\varepsilon_r}$
1GHz_TDSP	3.56	3.72	3.78	3.69
1GHz_SRM	2.50	3.18	2.00	2.56
2GHz_TDSP	3.67	3.67	4.00	3.78
2GHz_SRM	1.82	1.79	1.62	1.74
2GHz_NA_TDSP	1.57	3.73	4.00	3.87
2GHz_NA_SRM	1.82	1.68	1.64	1.66
VMF	3.64	3.64	3.64	3.64

Fig. 9. Processed values of the relative dielectric permittivity computed using the TDSP and the SRM methods for the acquisitions made with the 1000 MHz, 2000 MHz and 2000 MHz (NA) central-frequency antennas (dielectrics by the VMF method are also added).

7 CONCLUSION AND FUTURE PROSPECTS

This paper reports an extended study of applications of ground-penetrating radar (GPR) on the assessment of the electromagnetic (EM) properties of railway ballast.

The main geometric, physical and mechanical properties of clean limestone ballast aggregates are first assessed in the laboratory environment according to relevant standard test methods. A typical ballast layer of a track bed substructure is reproduced using a square-based methacrylate tank, with outer dimensions of 1.55 m length × 1,55 m width × 0.55 height. A copper sheet is placed beneath the tank to allow the complete reflection of the EM waves propagating through the material. The use of this perfect electric conductor (PEC) allows for the effective assessment of the EM properties of the material, which is the primary scope of this work. The container is filled up with the ballast aggregates and emptied several times in order to reproduce different scenarios of aggregates arrangement. Four GPR systems (in both ground-coupled and air-coupled configurations) investigating with five differing central frequencies are used for testing purposes. A processing scheme for filtering out useless information from the raw GPR data is developed.

The effects of the ringing and the low directivity of the ground-coupled antennas return lower dielectrics as opposed to the reference literature values of permittivity for railway ballast layers as well as to the dielectrics computed using the air-coupled systems. The main cause for this occurrence is linked to the roughness of the ballast aggregates at the top of the container that makes the interface between the air and the top aggregates highly irregular. These results may indicate unsuitability of the used ground-coupled system type for the railway ballast investigation carried out in this study.

With regard to the used antenna-frequencies (air-coupled systems), results show that the higher the central frequency of investigation, the larger the value of the permittivity computed by means of the time-domain signal picking (TDSP) method.

The application of the proposed data processing scheme return slightly higher values of dielectric permittivity than the raw, i.e., not exceeding ± 3%. This occurs across the investigated scenarios of aggregates arrangement as well as across the used frequencies of investigation.

The use of the surface reflection method (SRM) appears to be not suitable for the assessment of the relative dielectric permittivity of limestone railway ballast in clean conditions. This is due to a higher sensitivity of the SRM towards the roughness of the ballast aggregates at the interface between the air and the "ballast system" (i.e., effect on the reflection amplitude) in combination with the high inhomogeneity of the material throughout the investigated domain (i.e., loss of the major assumption of material homogeneity from the SRM method). On the contrary, a general agreement between the dielectrics computed with the TDSP and the VMF is observed. Overall, it can be seen how the permittivity assessed by the VMF is lower than the dielectrics derived from the application of the time-domain-based technique. In addition to this, lower mismatches are observed in the case of the 1000 MHz antenna, whereas the use of the 2000 MHz antennas (in both the standard and low-powered configurations) return broadly higher differences. The 2000 MHz (NA) frequency data processed with the TDSP technique return the largest difference with respect to the dielectrics computed using the VMF method.

With regard to the effects of the arrangement of the ballast aggregates on the dielectric permittivity (i.e., the variability observed in the values of the permittivity), a different disposition of the aggregates, surveyed by the same antenna, may affect the computed values of the permittivity of the "ballast system" more than using different frequencies of investigation across the same section (scenario).

In view of the above results, the 1000 MHz air-coupled antenna system seems to be the most reliable and stable GPR device (among the set of system types and frequencies used) for the purposes of this study. Indeed, the use of this antenna frequency system allows for the lowest differences in terms of permittivity before and after the application of the data processing scheme. The investigations performed with the 1000 MHz antenna frequency provides also with the smallest differences between the dielectrics computed using the TDSP technique and the VMF method. Furthermore, the permittivity data calculated with this frequency return the lowest changes across the three different scenarios of particles arrangement provided.

Future research could task itself with the applicability of the obtained findings to real-case scenarios. Due to the higher complexity of the investigation domain in terms of boundary conditions (e.g., presence of tracks/sleepers, fouling, moisture within the track bed etc.), it is recommended to carry out first a survey at the network level to divide the railway track into homogeneous stretches. This will allow to single out clean ballast areas where to utilize the GPR systems and indications arising from this study.

ACKNOWLEDGEMENTS

The authors are grateful to Mr. Spartaco Cera, from Roma Tre University, for providing invaluable help in the context of the experimental tests. Special thanks to IDS Georadar for supplying part of the GPR systems, and Clax Italia s.r.l. for manufacturing the methacrylate tank. This work has also benefited from the network activities carried out within the EU funded COST Action TU1208 "Civil Engineering Applications of Ground Penetrating Radar."

References

1. Clark MR, Gillespie R, Kemp T, McCann DM, Forde MC. Electromagnetic properties of railway ballast. NDTE Int 2001;34:305–11.
2. Roberts R, Al-Qadi I, Tutumluer E, Boyle J, Sussmann TR. Advances in railroad ballast evaluation using 2 GHz horn antennas. Proceedings of the 11th International Conference on Ground Penetrating Radar, Columbus, OH., USA, 2006.
3. Selig ET, Collingwood BI, Field SW. Causes of fouling in track. AREA Bulletin 1998;71.
4. Shao W, Bouzerdoum A, Phung SL, Su L, Indratatna B, Rujikiatkamjorn C. Automatic classification of ground-penetrating-radar signals for railway-ballast assessment. IEEE T Geosci Remote 2010;49(10):3961–72.
5. Cho GC, Dodds J, Santamaria JC. Particle shape effects on packing density, stiffness and strength of natural and crushed sands. J Geotech Geoenviron 2006;132(5):591-602.
6. Sun Y, Indraratna B, Nimbalkar S. Three-dimensional characterisation of particle size and shape for ballast. Géotechnique Letters 2014;4(3):197-202.
7. Tosti F, Pajewski L. Applications of radar systems in planetary sciences: an overview. Chapt. 15 - Civil Engineering Applications of GPR, Springer Trans. in Civ. and Environm. Eng. Book Series. 2015;361–371.
8. Benedetto A, Pajewski L. Civil Engineering Applications of Ground Penetrating Radar. Springer Transactions in Civil and Environmental Engineering Book Series, 2015.
9. Benson AK. Applications of ground penetrating radar in assessing some geological hazards: examples of groundwater contamination, faults, cavities. J Appl Geophys 2001:33(1-3);177–93.
10. Goodman D. Ground-penetrating radar simulation in engineering and archaeology. Geophysics 1994:59(2);224-32.
11. Schultz JJ, Collins ME, Falsetti AB. Sequential monitoring of burials containing large pig cadavers using ground-penetrating radar. J Foren Sci 2006:51(3);607-16.
12. Saarenketo T, Scullion T. Road Evaluation with Ground Penetrating Radar. J Appl Geophys 2000:43;119–38.

13. Al-Qadi IL, Lahouar S. Use of GPR for thickness measurement and quality control of flexible pavements. J Ass Asph Paving Technologists 2004:73;501–528.
14. Fauchard C, Dérobert X, Cariou J, and Côte P. GPR performances for thickness calibration on road test sites. NDTE Int 2003:36(2);67-75.
15. Loizos A, Plati C. Accuracy of pavement thicknesses estimation using different ground penetrating radar analysis approaches. NDTE Int 2007:40(2);147-157.
16. Tosti F, Adabi S, Pajewski L, Schettini G, Benedetto A. Large-scale analysis of dielectric and mechanical properties of pavement using GPR and LFWD. in Proceedings of the 15th International Conference of Ground Penetrating Radar (GPR 2014), Brussels, Belgium, Jun. – Jul. 2014, Paper no. 6970551, pp. 868-873.
17. Benedetto A, Tosti F. Inferring bearing ratio of unbound materials from dielectric properties using GPR: the case of Runaway Safety Areas. In Proceedings of the Airfield and Highway Pavement 2013: Sustainable and Efficient Pavements, Los Angeles, USA, June 2013, pp. 1336–1347.
18. Patriarca C, Tosti F, Velds C, Benedetto A, Lambot S, Slob EC. Frequency dependent electric properties of homogeneous multi-phase lossy media in the ground-penetrating radar frequency range. J Appl Geophys 2013: 1(97); 81–88.
19. Tosti F, Benedetto A, Bianchini Ciampoli L, Lambot S, Patriarca C, Slob EC. GPR analysis of clayey soil behaviour in unsaturated conditions for pavement engineering and geoscience applications. Near Surf Geophys 2016:14(2);127-144.
20. Al-Qadi IL, Lahouar S. Measuring rebar cover depth in rigid pavements with ground-penetrating radar. Transp Res Rec 2005: 1907; 81-85.
21. Benedetto A, Tosti F, Ortuani B, Giudici M, Mele M. Mapping the spatial variation of soil moisture at the large scale using GPR for pavement applications. Near Surf Geophys 2015:13(3);269-278.
22. Benedetto F, Tosti F. GPR spectral analysis for clay content evaluation by the frequency shift method. J Appl Geophys 2013:1(97);89–96.
23. Jørgensen AS, Andreasen F. Mapping of permafrost surface using ground-penetrating radar at Kangerlussuaq Airport, western Greenland. Cold Reg Sci Technol 2007:48(1);64–72.

24. Benedetto A, Manacorda G, Simi A, Tosti F. Novel perspectives in bridge inspections using GPR. Nondestruct Test Eva 2012:27(3);239–251.
25. Alani AM, Aboutalebi M, Kilic G. Applications of ground penetrating radar (GPR) in bridge deck monitoring and assessment. J Appl Geophys 2013:97;45-54.
26. Alani AM, Banks K. Applications of ground penetrating radar in the Medway Tunnel - Inspection of structural joints. In Proceedings of the 15th International Conference of Ground Penetrating Radar (GPR 2014), Brussels, Belgium, Jun. – Jul. 2014, art. no. 6970466, pp. 461–464.
27. Roberts R, Schutz A, Al-Qadi IL, Tutumluer E. Characterizing railroad ballast using GPR: recent experiences in the United States. In Proceedings of the 2007 4th International Workshop on Advanced Ground Penetrating Radar (IWAGPR 2007), Naples, Italy, 2007, pp. 295–299.
28. Railway Track and Structures Magazine, June 1985.
29. Hugenschmidt J. Railway track inspection using GPR. J Appl Geophys 2000:43(2-4);147–55.
30. Olhoeft GR, Selig ET. Ground penetrating radar evaluation of railroad track substructure conditions. In Proceedings of the 9th International Conference on Ground Penetrating Radar (GPR 2002), Santa Barbara, USA, Apr. – May 2002.
31. Leng Z, Al-Qadi IL. Railroad ballast evaluation using ground-penetrating radar. Transp Res Rec 2010:2159;1110–17.
32. Sussmann TR, O'Hara KR, Selig ET. Development of material properties for railway application of ground penetrating radar. In Proceedings of the Society of Photo-Optical Instrumentation Engineers (SPIE), vol. 4758, 2002.
33. De Chiara F. Improvement of railway track diagnosis using ground penetrating radar. PhD Thesis, 2014.
34. Tosti F, Patriarca C, Slob E, Benedetto A, Lambot S. Clay content evaluation in soils through GPR signal processing. J Appl Geophys 2013:97;69-80.
35. Redman J, Davis J, Galagedara L, Parkin G. Field studies of GPR air launched surface reflectivity measurements of soil water content. In Proceedings of the 9th International Conference on Ground Penetrating Radar (GPR 2002), Santa Barbara, California, USA, 2002, art. no. 4758, pp. 156-161.
36. ASTM D6087-08. Standard Test Method for Evaluating Asphalt-Covered Concrete Bridge Decks Using Ground Penetrating Radar. ASTM International, West Conshohocken, PA, 2008.

561 37. F. Benedetto, F. Tosti, A signal processing methodology for assessing the performance of ASTM standard
562 test methods for GPR systems, Signal Process. 132 (2017) 327–337.
563 38. Pramudita.A.A, Kurniaawal.A,Suksmono.A.B, Lestari.A.A, "Effect of antenna dimensions on the
564 antenna footprint in ground penetrating radar applications," Microwaves, IET Antennas & Propagation,
565 IET.Volume:3 , Issue: 8, pp.1271 - 1278 ,2009
566 39. Birchak JR, Gardner CG, Hipp JE, Victor JM. High dielectric constant microwave probes for sensing soil
567 moisture. In Proceedings of the IEEE 62, (1974) 93–102.
568 40. West, L. J., K. Handley, Y. Huang, and M. Pokar, "Radar frequency dispersion in sandstone: Implication
569 for determination of moisture and clay content," Water Resources Research, Vol. 39, 1026, 2003.
570 41. Roth, K., R. Schulin, H. Fluher, and W. Attinger, "Calibration of time-domain reflectometry for water
571 content measurement using a composite dielectric approach," Water Resources Research, Vol. 26, No.
572 10, 2267–2273, 1990.
573 42. Lichtenecker, K., Rother, K., 1931. Die herleitung des logarithmischen mischungsgesetzes aus
574 allgemeinen prinzipien der stätionaren strömung. Physik Z. 32, 255–260.
575 43. Zakri, T., J. P. Laurent, and M. Vauclin, "Theoritical evidence for 'Lichtenecker's mixture formulae,'
576 based on effective medium theory," Journal of Physics D: Applied Physics, Vol. 31, 1589– 1594, 1998.
577 44. Brovelli, A. and G. Cassiani, "Effective permittivity of porous media: A critical analysis of the complex
578 refractive index model," Geophysical Prospecting, Vol. 56, 715–727, 2008.
579 45. Fensler WE, Knott EF, Olte A, Siegel KM. The electromagnetic parameters of selected terrestrial and
580 extraterrestrial rocks and glasses. The moon, (Kopal, Z., and Mikhailov, Z.K., Ed) IAU Symposium 14,
581 545-565.
582 46. Annan AP. Practical processing of GPR data, Sensors and Software Inc., 1999.
583 47. Jol H. Ground Penetrating Radar, Ed. Elsevier, 2009.
584 48. Yelf R, Yelf D. Where is true time zero? Electromagn Phenom 2006:71(18);159–63.
585 49. Benedetto A, Tosti F, Bianchini Ciampoli L, D'Amico F. An overview of ground-penetrating radar signal
586 processing techniques for road inspections. Signal Process 2017:132;201-209.

587 50. Pajewski L, Tosti F, Kusayanagi W. Antennas for GPR Systems. Chapter 2 - Civil Engineering
588 Applications of Ground Penetrating Radar, Springer Transactions in Civil and Environmental Engineering
589 Book Series, 41–67, 2015.
590 51. Benedetto A, Tosti F, Bianchini Ciampoli L, Calvi A, Brancadoro MG, Alani AM. Railway ballast
591 condition assessment using ground-penetrating radar – an experimental, numerical simulation and
592 modelling development. Constr Build Mater 2016;140:508–20.
593 52. Bianchini Ciampoli L, Tosti F, Brancadoro MG, D'Amico F, Alani AM, Benedetto A. A spectral analysis
594 of ground-penetrating radar data for the assessment of the railway ballast geometric properties. NDTE Int
595 2017:90; 39-47.
596 53. D.J. Daniels, Ground Penetrating Radar, The Institution of Electrical Engineers, London, 2004.
597 54. Federal Communications Commission Office of Engineering & Technology. 1997. Evaluating
598 Compliance with FCC Guidelines for Human Exposure to Radiofrequency Electromagnetic Fields, *OET*
599 *Bulletin 65, Edition 97-01*.
600 55. Bianchini Ciampoli, L., D'Amico, F., Calvi, A., Benedetto, F. and **Tosti, F.** (2017). Signal processing for
601 optimisation of low-powered GPR data with application in transportation engineering (roads and
602 railways). In: *Proc. of the Tenth International Conference on the Bearing Capacity of Roads, Railways*
603 *and Airfields (BCRRA 2017)*, June 28-30, Athens, Greece. https://doi.org/10.1201/9781315100333-223
604 56. EN 13450:2002/AC:2004. Aggregates for railway ballast. Europ. Comm. for Standardization, 2004.
605 57. EN 1097-3:1998. Tests for mechanical and physical properties of aggregates - Part 3: Determination of
606 loose bulk density and voids. Europ. Comm. for Standardization, 1998.
607 58. CEN ISO/TS 17892-1:2014. Geotechnical investigation and testing - Laboratory testing of soil - Part 1:
608 Determination of water content (ISO 17892-1:2014). Europ. Comm. for Standardization, 2014.
609 59. EN 933-1:2012. Tests for geometrical properties of aggregates - Part 1: Determination of particle size
610 distribution -Sieving method. Europ. Comm. for Standardization, 2012.
611 60. EN 933-4:2008. Tests for geometrical properties of aggregates - Part 4: Determination of particle shape -
612 Shape index. European Committee for Standardization, 2008.
613 61. EN 1097-2:2010. Tests for mechanical and physical properties of aggregates - Part 2: Methods for the
614 determination of resistance to fragmentation. Europ. Comm. for Standardization, 2010.

62. EN1097-6:2013. Tests for mechanical and physical properties of aggregates-Part 6:Determination of particle density and water absorption. Europ Comm for Stand, 2013.
63. Narayanan RM, Kumke CJ, Li D. Railroad track monitoring using ground penetrating radar: simulation study and field measurements. In: SPIE conference on subsurface sensors and applications, 1999, p. 3752.
64. Al-Qadi IL, Xie W, Roberts R. Scattering analysis of ground-penetrating radar data to quantify railroad ballast contamination. NDT&E Int 2008:41;441-47.
65. Lambot S, Antoine M, Vanclooster M, Slob EC. Effect of soil roughness on the inversion of off-ground monostatic GPR signal for noninvasive quantification of soil properties. Water Resour Res 2006:42(3).
66. Reynolds, J.M., 1997, An lntroduction to Applied and Environmental Geophysics, John Wiley and Sons, Chichester.